ELSEVIER

Journal of Power Sources 81–82 (1999) 616–620

JOURNAL OF POWER SOURCES

www.elsevier.com/locate/jpowsour

In situ Raman spectroscopic studies of electrochemical intercalation in $Li_xMn_2O_4$-based cathodes

Weiwei Huang [1], Roger Frech *

Department of Chemistry, University of Oklahoma, Norman, OK 73019 USA

Abstract

Raman spectra of spinel $Li_xMn_2O_4$ ($x = 1.0$ and 1.1) were recorded in situ during electrochemical intercalation of lithium ions. We demonstrate that phases and structural modifications in these compounds can be identified using Raman spectroscopy. In stoichiometric $LiMn_2O_4$, Raman spectral results indicated that a single-phase reaction is followed by a two-phase reaction and then by another single phase reaction when lithium is deintercalated from the spinel compound ($0.1 < x < 1.0$). In nonstoichiometric $Li_xMn_2O_4$ ($x = 1.1$), Raman spectra clearly identify the presence of the λ-MnO_2 phase in the cathode during charge and discharge. When spinel $LiMn_2O_4$ was intercalated with lithium ions, the in situ Raman spectral changes were consistent with a two-phase reaction between cubic $LiMn_2O_4$ and tetragonal $Li_2Mn_2O_4$.

Keywords: $Li_xMn_2O_4$-based cathodes; Raman spectroscopy; Electrochemical intercalation

1. Introduction

Spinel $Li_xMn_2O_4$ has been used in commercial lithium-ion cells [1]. Although the capacity of spinel $Li_xMn_2O_4$ is lower than that of $LiCoO_2$, the low cost and low toxicity of $Li_xMn_2O_4$ make it an attractive cathode material. It is known that during charge/discharge cycling in the potential range of 3.0 to 4.2 V vs. Li/Li^+, stoichiometric $LiMn_2O_4$ spinel shows significant capacity-fade, which is attributed to several factors [2], including dissolution of manganese from the spinel electrodes, oxidation of electrolytes, and a structural change due to Jahn–Teller distortion of the cubic spinel in the discharged state.

The structural changes of stoichiometric $LiMn_2O_4$ spinel during charge and discharge have been characterized mainly by X-ray [3–8], neutron power diffractometry [8] and FTIR spectroscopy [9,10]. Based on X-ray diffraction data of spinel $Li_xMn_2O_4$ recorded ex situ during lithium intercalation, Ozhuku et al. reported the coexistence of two cubic phases for $0.27 < x < 0.60$, the presence of a single phase for $0.60 < x < 1.0$, and the coexistence of a cubic and a tetragonal phase for $1.0 < x < 2.0$ [3]. Liu et al. [8] examined the structural changes in the 4-V regions using ex situ X-ray and neutron diffraction techniques and proposed a slightly different mechanism for the structural changes of $Li_xMn_2O_4$ during electrochemical intercalation. They stated that charged $Li_xMn_2O_4$ exists as a single-phase structure (λ-MnO_2) for $0 < x < 0.10$, then enters a coexistence region of two cubic phases for $0.20 < x < 0.35$, followed by a single cubic phase region for $0.35 < x < 0.50$ and another cubic phase region for $0.50 < x < 1.0$. FTIR results by Richardson et al. [9], by Wen et al. [10] and by Huang and Frech [11] showed distinct bands for cubic $LiMn_2O_4$ and tetragonal $Li_2Mn_2O_4$, but could not clearly identify different cubic phases of $Li_xMn_2O_4$ when x is varied from 0.1 to 1.0.

Recently, it has been shown that if the starting $Li_xMn_2O_4$ compound contains a small amount of excess lithium or oxygen with respect to the stoichiometric $LiMn_2O_4$, it will considerably reduce the capacity fade [4,11,12]. Xia and Yoshio [4] performed ex situ X-ray diffraction studies of both stoichiometric $LiMn_2O_4$ and nonstoichiometric $Li_{1+x}Mn_2O_{4+y}$ and reported a two-phase reaction for the stoichiometric spinel in the range of $0.1 < x < 0.45$ but a one-phase reaction for the nonstoichiometric spinel in the entire intercalation range investigated ($0.25 < x1.04$). They attributed the better cycle life of nonstoichiometric $Li_{1+x}Mn_2O_{4+y}$ ($x \geq 0$, $y > 0$) to this one-phase reaction mechanism. In situ X-ray diffraction results reported by Amatucci et al. [5] and Mukerhee et al.

* Corresponding author

[1] Current address: Eveready Battery, 25225 Detroit Road, Westlake, OH 44145, USA.

0378-7753/99/$ - see front matter
PII: S0378-7753(99)00231-1

[6] also indicated the coexistence of two phases for stoichiometric $LiMn_2O_4$ between $x = 0.20$ to 0.45 and a suppressed two-phase coexistence for the nonstoichiometric $Li_{1+x}Mn_2O_{4+y}$ during charge and discharge.

In this work, we report the in situ Raman spectroscopic studies of both stoichiometric $LiMn_2O_4$ and nonstoichiometric $Li_{1.1}Mn_2O_4$ during charge and discharge. Since Raman spectroscopy has proved to be a convenient and powerful structural technique in our previous in situ work on $Li_xV_2O_5$ [13] and synthetic graphite [14] during electrochemical reaction, we naturally extended our studies to $Li_xMn_2O_4$ which is a commercial cathode for lithium ion cells. Others have also used the in situ Raman technique to examine structural changes in electrode materials, including Li_xCoO_2 [15], the lithium surface [16,17], and a pioneering study of highly oriented pyrolytic graphite [18]. Kanoh et al. [19] studied lithium ion electroinsertion in a Pt/λ-MnO_2 electrode in aqueous solution using in situ Raman spectroscopy. The purpose of this study is to further demonstrate the usefulness of Raman scattering technique for in situ studies of structural changes of electrodes in general and to examine the complicated phase changes of $Li_xMn_2O_4$ during lithium intercalation process in particular.

2. Experimental

Samples of spinel $LiMn_2O_4$ and $Li_{1.1}Mn_2O_4$ were synthesized using a method very similar to that described by Tarascon et al. [20]. Ball-milled mixtures of Li_2CO_3 and MnO_2 were first heated in a Lindberg furnace at 750°C for 24 h and then cooled to room temperature after the furnace was switched off. The samples were then subjected to hand grinding and a heating–cooling sequence identical to the first heating-cooling process. Tetragonal $Li_2Mn_2O_4$ was prepared from reaction of $LiMn_2O_4$ with LiI in heated acetone solution according to the method described by Tarascon and Guyomard [21]. The cathode electrode films which were cast from cyclopentanone solutions consisted of 85 wt.% active cathode material, 10 wt.% Super-P and 5 wt.% polyvinylidene. The prepared films were then pressed onto aluminum meshes and dried at 120°C under vacuum for 12 h before use.

Two-electrode (cathode and lithium metal) cells were assembled in a dry box filled with ultrahigh-purity argon gas. A 1 M $LiClO_4$ solution of a 1:1 (weight ratio) mixture of ethylene carbonate–dimethyl carbonate and Celgard® 2400 was used as the electrolyte and separator, respectively. Cells were charged and discharged using an EG&G potentiostat/galvanostat (Model 263) at a constant current density of 0.3 mA/cm^2.

In situ Raman spectral data were collected at room temperature using the microscope attachment of a Jobin-Yvon ISA T64000 Raman spectrometer equipped with a charge coupled device (CCD) detector and a TV monitor to observe sample surface images. The 80 × objective lens of the microscope was used to focus the laser beam on a small selected area (about 1 μm^2) of the cathode surface, and the backscattered Raman signal was collected. The Raman excitation source was the 514.5 nm line of a Lexel argon ion laser excited at 20 mW. In a typical spectral acquisition, which took about 2 min, five Raman spectra each recorded over the frequency range of 180 to 840 cm^{-1} at an acquisition time of 16 s, were averaged to increase the single-to-noise ratio. The schematic drawing of the spectroelectrochemical cell used in this study can be found in Ref. [14].

3. Results and discussion

Fig. 1 shows the potential curves of stoichiometric $LiMn_2O_4$ during the first charge and discharge in the potential range of 4.60 to 2.85 V vs. Li/Li$^+$. The charged capacity was 141 mAh/g for the cathode and matched well with the published data by others [7,8]. The discharge capacity to 2.85 V was only 115 mAh/g after the cell had been charged to 4.60 V, indicating some capacity loss. A plateau at 3.15 V in the discharge potential curve was observed, although it was absent in the first charge curve. The cause of this plateau is unknown at present but is related to the 4.5 plateau in the first charge potential curve as pointed by Gao and Dahn [22].

In situ Raman spectra of $Li_xMn_2O_4$ during the first charge were shown in Fig. 2a. Only a weak band at 631 cm^{-1} and a shoulder at 609 cm^{-1} were observed at $x = 1.0$, although the stoichiometric spinel compound $LiMn_2O_4$ has five Raman vibrational bands ($A_{1g} + E_g + 3F_{2g}$) at the Brillouin zone center. When the cell potential increased from 2.97 to 4.00 V, the shoulder gradually disappeared whereas the band at 631 cm^{-1} remained unchanged. As the cell potential further increased from 4.00 to 4.12 V, a new band appeared at 596 cm^{-1} and grew in intensity at the expense of the band at 631 cm^{-1}. The coexistence of these two bands is an indication of coexistence of two structural phases for the spinel in this

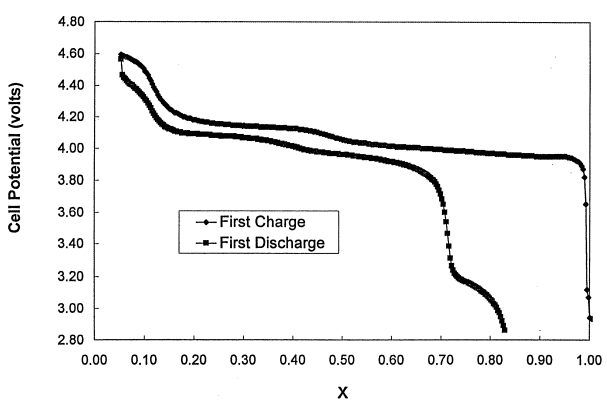

Fig. 1. The potential curves for stoichiometric $LiMn_2O_4$ between 2.85 and 4.6 V during the first charge and discharge (0.3 mA/cm^2).

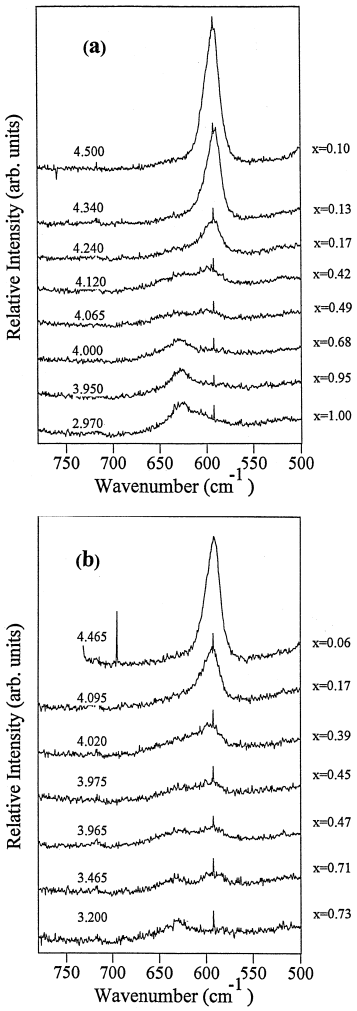

Fig. 2. In situ Raman spectra of stoichiometric $LiMn_2O_4$ ($0 < x < 1$) in the frequency interval 500 to 775 cm^{-1} during the first charge (a) and discharge (b). The numbers on the figure are the cell potential in volts. The frequency shift of the spike in the Raman spectrum recorded at 4.465 V in (b) was due to a different frequency window used for recording this spectrum.

potential range. The new band, attributed to the formation of the λ-MnO_2 phase, became the only Raman band when the cell potential reached 4.24 volts and showed a dramatic increase in intensity as the cell was further charged to 4.50 V. These Raman spectral changes were consistent with results from X-ray studies, i.e., a single-phase reaction followed by a two-phase reaction and then by a single-phase reaction when lithium is deintercalated from the spinel $LiMn_2O_4$ [3,4,8]. The dramatic increase in Raman intensity at potentials over 4.24 V is probably related to the decrease of the electronic conductivity [15] of $Li_xMn_2O_4$ as x approaches zero. However,it should be noted that this explanation is in contrast to the conductivity data measured by Pistoia et al. who reported that the conductivity was slightly increased from 2×10^{-6} S/cm for $LiMn_2O_4$ to 3×10^{-6} S/cm for λ-MnO_2 [23].

When λ-MnO_2 was discharged from 4.60 to 2.90 V, the Raman spectral behavior was the reverse of that observed during the initial charge process (Fig. 2b), as expected. However, the Raman band at 596 cm^{-1} which was assigned to λ-MnO_2 phase was still observable even at 3.47 V. This may be due to the local inhomogeneity of the composite cathode, in which some regions exhibit a slow transition of the lambda phase to other phases. However, this λ-MnO_2 band disappeared as the cell potential was further decreased.

When the freshly prepared $LiMn_2O_4$ was discharged, a new band appeared at 614 cm^{-1} and grew in intensity at the expense of the $LiMn_2O_4$ band at 631 cm^{-1} as the cell potential decreased (Fig. 3a). The coexistence of this new band with the band at 631 cm^{-1} is consistent with the two-phase reaction mechanism in this potential range [3]. When the cell potential reached 2.10 V, the discharge

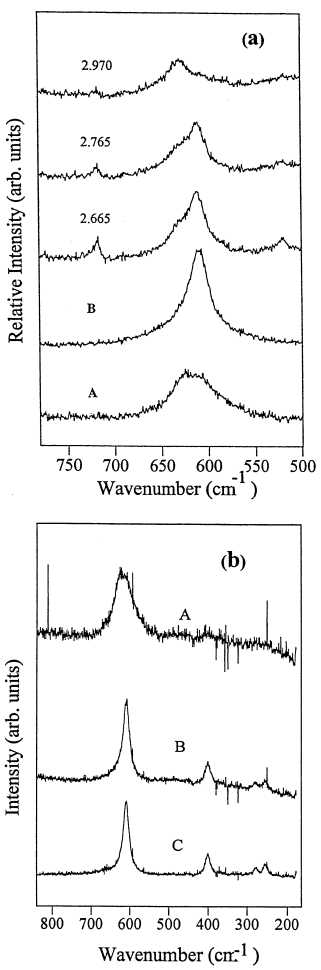

Fig. 3. In situ Raman spectra of stoichiometric $Li_xMn_2O_4$ ($1 < x < 2$) in the frequency interval (a) 500 to 775 cm^{-1} and (b) 180 to 840 cm^{-1} during the first discharge. The numbers on the figure are the cell potential in volts. In (a), curves A and B are Raman bands from domains with gray-black and orange colors, respectively. In (b), A and B are Raman spectra corresponding to gray-black and orange colored domains; C is from chemically prepared $Li_2Mn_2O_4$.

process was terminated and the cell was disassembled. The scratched surface of the Li_xMnO_4 electrode appeared to consist at least two types of micro-domains, which were orange and gray-black in color. The orange-colored micro-domains, like the chemically synthesized tetragonal $Li_2Mn_2O_4$, showed an intense band at 611 cm^{-1} and three other weak bands at 400, 278, and 259 cm^{-1} (Fig. 3b) whereas the gray-black colored spots contributed two bands at 628 and 609 cm^{-1} which were due to major bands of cubic $LiMn_2O_4$ and tetragonal $Li_2Mn_2O_4$, respectively.

Fig. 4 shows the first charge and discharge potential curves in the range of 4.8 to 3.0 V for nonstoichiometric $Li_xMn_2O_4$ ($x = 1.1$). The charged capacity to 4.8 V was 100 mAh/g, lower than that of the stoichiometric $LiMn_2O_4$, as expected. There was no 3.3-V plateau in the discharge potential curve although the cell had been charged to 4.8 V, similar to results reported by Gao and Dahn [22].

In situ Raman spectral changes of nonstoichiometric $Li_xMn_2O_4$ ($x = 1.1$) during the first charge are shown in Fig. 5. The Raman bands of the pristine $Li_{1.1}Mn_2O_4$ were very weak and could not be easily identified. The bands at 720 and 521 cm^{-1} were solvent bands whereas the broad band centered at 632 cm^{-1} was due to both $Li_{1.1}Mn_2O_4$ and solvent. As the cell potential was raised to 4.04 V a new band started to appear at 597 cm^{-1} and increased in intensity as the cell was further charged to 4.63 V. This band is assigned to λ-MnO_2 in the cathode because it occurs at the same frequency and exhibits the same intensity behavior as the λ-MnO_2 formed in $LiMn_2O_4$ during charge and discharge. It should be noted that there is some lithium present in the λ-MnO_2 phase (see Fig. 4); consequently, this phase is sometimes denoted as λ-Li_xMnO_2 in the literature [24]. When the spinel compound was discharged from 4.80 to 2.97 V, the observed spectral changes were the reverse of those observed during the initial charge process and the spectra are omitted here. In contrast to the X-ray studies which showed either a continuous reaction [4] over the entire intercalated range of $0.25 < x < 1.04$ or a suppressed two-phase coexistence [6] in the intercalation

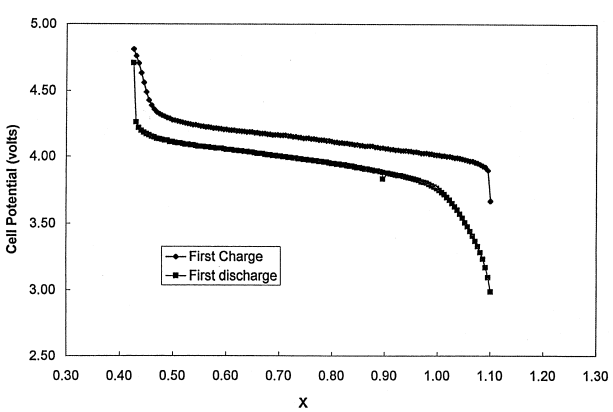

Fig. 4. The potential curves for nonstoichiometric $Li_{1.1}Mn_2O_4$ between 3.0 and 4.8 V during the first charge and discharge (0.3 mA/cm^2).

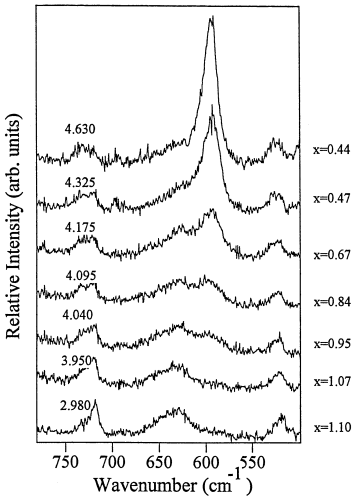

Fig. 5. In situ Raman spectra of nonstoichiometric $Li_{1.1}Mn_2O_4$ in the frequency interval 500 to 775 cm^{-1} during the first charge.

ranges of $x = 0.45$ to 0.20, our Raman spectra could clearly identifies the appearance of the λ-MnO_2 phase during the charge or discharge of nonstoichiometric $Li_xMn_2O_4$.

4. Conclusion

A weak band at 631 cm^{-1} and a shoulder at 609 cm^{-1} were observed for the stoichiometric spinel compound $LiMn_2O_4$, although it is predicted to have five Raman active vibrational bands at the Brillouin zone center. The in situ Raman spectral changes indicated that a single-phase reaction is followed by a two-phase reaction and then by another single phase reaction as lithium ions are deintercalated from stoichiometric $LiMn_2O_4$. The λ-MnO_2 phase, formed in both the stoichiometric and nonstoichiometric $Li_xMn_2O_4$ during charge and discharge, has a distinct band at 597 cm^{-1} and therefore can be easily identified from the Raman spectra. When spinel $LiMn_2O_4$ is intercalated with lithium, the in situ Raman spectral changes are consistent with a two-phase reaction between cubic $LiMn_2O_4$ and tetragonal $Li_2Mn_2O_4$. The tetragonal $Li_2Mn_2O_4$ phase shows an intense band at 611 cm^{-1} and three other weak bands at 400, 278, and 259 cm^{-1}, which provide a useful spectroscopic 'fingerprint' for the identification of this phase.

Acknowledgements

This work was supported by funds from the U.S. Army Research Office (Grant no. DAAG55-98-1-0252) and NSF EPSCoR program (Cooperative Agreement No. OSR-9559478).

References

[1] U. Von Sacken, The 15th Intl. Seminar and Exhibit on Primary and Secondary Batteries, Fort Lauderdale, FL, USA, March 2–5, 1998.
[2] M.M. Thackery, Prog. Solid State Chem. 25 (1997) 1, and references therein.
[3] T. Ohzuku, M. Kitagawa, T. Hirai, J. Electrochem. Soc. 137 (1990) 769.
[4] Y. Xia, M. Yoshio, J. Electrochem. Soc. 143 (1996) 825.
[5] G. Amatucci, J.M. Tarascon, C. Schmultz, D. Karcher, A.S. Gozdz, F. Shokoohi, Abstract 47, The Electrochemical Society Meeting Abstracts, Vol. 96-1, Los Angeles, CA, May 5–10, 1996, p. 57.
[6] S. Mukerjee, T.R. Thurston, N.M. Jisrawi, X.Q. Yang, J. McBreen, M.L. Daroux, X.K. Xing, J. Electrochem. Soc. 145 (1998) 466.
[7] M.N. Richard, I. Koetschau, J.R. Dahn, J. Electrochem. Soc. 144 (1997) 554.
[8] W. Liu, K. Kowal, G.C. Farrington, J. Electrochem. Soc. 145 (1998) 459.
[9] T.J. Richardson, S.J. Wen, K.A. Striebel, P.N. Ross Jr., E.J. Cairns, Mater. Res. Bull. 32 (1997) 609.
[10] S.J. Wen, T.J. Richardson, L. Ma, K.A. Striebel, P.N. Ross Jr., E.J. Cairns, J. Electrochem. Soc. 143 (1996) L136.
[11] W. Huang, R. Frech, Unpublished results.
[12] J.R. Tarascon, F. Coowar, G. Matuci, F.K. Shokoohi, D.G. Guyomard, J. Power Sources 54 (1995) 103.
[13] X. Zhang, R. Frech, J. Electrochem. Soc. 145 (1998) 847.
[14] W. Huang, R. Frech, J. Electrochem. Soc. 145 (1998) 765.
[15] T. Itoh, H. Sato, T. Nishina, T. Matue, I. Uchida, J. Power Sources 68 (1997) 333.
[16] M. Odziemkowski, M. Krell, D.E. Irish, J. Electrochem. Soc. 139 (1992) 3052.
[17] T. Itoh, Y. Matsutani, I. Uchida, Denki Kagaku 64 (1996) 76.
[18] M. Inaba, H. Yoshida, Z. Ogumi, T. Abe, Y. Mizutani, M. Asano, J. Electrochem. Soc. 142 (1995) 20.
[19] H. Kanoh, W. Tang, K. Ooi, Electrochem. Solid State Lett. 1 (1998) 17.
[20] J.M. Tarascon, W.R. McKinnon, F. Coowar, T.N. Bowmer, G. Amatucci, D. Guyomard, J. Electrochem. Soc. 141 (1994) 1421.
[21] J.M. Tarascon, D. Guyomard, J. Electrochem. Soc. 138 (1991) 2864.
[22] Y. Gao, J.R. Dahn, J. Electrochem. Soc. 143 (1996) 100.
[23] G. Pistoia, D. Zane, Y. Zhang, J. Electrochem. Soc. 142 (1995) 2551.
[24] J.M. Tarascon, E. Wang, F.K. Shokoohi, W.R. McKinnon, S. Colson, J. Electrochem. Soc. 138 (1991) 2859.